Check for updates

Identification of carbon deposition and its removal in solid oxide fuel cells by applying a non-conventional diagnostic tool

Vanja Subotić, [ID] *[a] Philipp Harter,[a] Mihails Kusnezoff,[b] Teko W. Napporn, [ID] [c] Hartmuth Schroettner[d] and Christoph Hochenauer[a]

Operating solid oxide fuel cells (SOFC) in a specific industry-relevant environment can result in undesired performance alterations and subsequent morphological changes. Conventional characterization tools, such as polarization curve or electrochemical impedance spectroscopy, can be employed to gain a rough overview of the cell performance. Nevertheless, if these conventional tools fail and seemingly invisible degradation mechanisms occur inside the cell and system, such degradation cannot be identified. Eventually, these mechanisms can cause the system to collapse abruptly and irreversibly. In this study, novel online-monitoring tools based on total harmonic distortion analysis (THD) were employed to identify the most relevant degradation mechanism when using carbon-containing fuels, *i.e.* carbon deposition. The examination was performed on SOFCs of industrial size, methane was used as a fuel, and the cells were operated under a constant current load. The operating conditions were designed as required for application in auxiliary power units (APUs). The results reveal that the preliminary stage of degradation can be most quickly identified using the frequencies: 1 Hz, 10 Hz, 100 Hz, 2 kHz, 2.5 kHz, 4 kHz and 8 kHz. If the lower frequencies are removed and only the frequencies equal to or higher than 2 kHz are applied, almost the same information is obtained, and the measuring time can be significantly reduced. In addition, this study enabled us to identify a highly efficient strategy that can be used to remove carbon and to regain the initial cell performance. Carbon removal during the regeneration process was also successfully detected by applying the THD methodology.

1 Introduction

Solid oxide fuel cells (SOFCs) offer attractive options to meet the rapidly increasing demand for emission-free energy supply systems. Used in a wide range of different technologies, the use of these cells results in high levels of electrical efficiency and very high levels of overall efficiency. SOFCs can be used effectively in applications in which the excess heat can be used to co-generate electricity and process heat. Moreover, they represent an excellent option in portable power and transportation applications, and especially for the power supply of large trucks.[1] However, the commercialization of SOFCs is still in its infancy, and several issues must still be addressed. All stack and system manufacturers are currently facing the same challenges in terms of system costs, reliability, durability and the validation of the system longevity for periods of more than 40 000 h.

To ensure the reliability of SOFCs, it is crucially important to answer the question "How close to their limits can SOFCs be operated?" This question is also of interest because the answers rely upon the limits defined. On the one hand, operating limits are defined as the capacity of the system to tolerate impurities, such as sulfur or chlorine. On the other hand, these operating conditions are selected by defining a system operator, such as the fuel type and operating current. The system tolerance level regarding impurities in both the fuel and oxidant is a decisive factor, which has been insufficiently investigated in SOFC systems. These impurities can also cause SOFC degradation and lead to a total system collapse. Local electrochemical deactivation, resulting from the poisoning and material degradation of an SOFC, occurs on both the nano- and micro-scales. Taking this aspect into consideration, the stack electrochemical activity increases at a specific macro-scale point; this activity, in turn, accelerates material degradation processes due to the increase in temperature. This effect can also result in several types of critical mechanical failures within the stack. Among the different fuel impurities, sulfur is well-known to cause the deactivation of catalytic active sites and decrease cell

[a]*Institute of Thermal Engineering, Graz University of Technology, Inffeldgasse 25/B, 8010 Graz, Austria. E-mail: vanja.subotic@tugraz.at; Fax: +43 316 8737305; Tel: +43 316 8737319*

[b]*Fraunhofer Institute for Ceramic Technologies and Systems IKTS, Winterbergstrasse 28, 01277 Dresden, Germany*

[c]*University of Poitiers, rue Michel Brunet B27 TSA 51106, 86073 Poitiers Cedex 09, France*

[d]*Institute for Electron Microscopy and Nanoanalysis, Graz University of Technology, Steyrergasse 17, 8010 Graz, Austria*

performance.[2–5] The critical concentration of sulfur in a fuel has a threshold of only 1 ppm in SOFC systems.[6] In addition, acidic gases, such as chlorine[7,8] and alkalic substances, should be removed from a fuel before it is used in an SOFC.[9] By ensuring that the appropriate fuel pre-processing steps are followed, system degradation due to fuel impurities can be properly controlled.

Aiming to increase the overall system efficiency, it seems to be necessary to reach the system operating limits in specific cases. In such cases, however, operation malfunctions can occur, and several failure modes can arise either independently or simultaneously. A good example of a failure mode is that of high fuel utilization. Most stack developers suggest that the stack should be operated at a fuel utilization rate of 60–85%.[10–12] A fuel utilization rate of even 94% has been reported,[13] although the authors of this study reported that a very low power density of 0.17 W cm^{-2} was achieved when using a 60/40 H$_2$/N$_2$ fuel mixture. However, even very tiny changes in fuel utilization can affect the system performance noticeably over longer periods of time. High fuel utilization can cause both macroscopic and microscopic changes in the SOFCs used. In a related study, a five-cell stack manufactured at Forschungszentrum Jülich GmbH was tested under high fuel utilization (90%) conditions.[14] The results show that the stack operation under such conditions caused the cells to oxidize locally. The greatest amount of oxidation was observed near the fuel outlet. Two different stack designs were employed, and 20% humidified fuel and pre-reformed liquified natural gas (LNG) were used. Both stacks operated smoothly under 85% fuel utilization conditions, although the initial effects of increasing the concentration polarization were already visible at 80% conditions. Very high fuel utilization leads to undesired Ni reoxidation effects, but also accelerated Ni agglomeration.[15] One possible way to increase the cell stability when operating under high fuel utilization conditions is to use alternative materials or anodes impregnated with noble metal catalysts.[16,17] Their applicability has already been approved for small button cells, but has not yet been approved for the industrial-sized cells. For this reason, it is necessary to make a compromise between achieving high fuel utilization or high power. In this context, the degradation caused by fuel shortages and the subsequent oxidation observed at the anode when higher amounts of fuel are utilized show how SOFCs work almost perfectly within the defined limits, but once these limits are exceeded, catastrophic consequences (e.g. regarding their durability) can occur. Therefore, a good compromise between durability and performance must be found, as SOFC systems need to be able to fulfill the high requirements placed on them and still operate effectively and efficiently.

When further considering the operating conditions that result from certain system operators, the steam/carbon-ratio (S/C) can be identified as an important parameter that can significantly influence the system longevity. Higher amounts of carbon-containing fuel components impact the carbon deposition processes. This eventually blocks porous gas channels or results in catalyst degradation.[18] Carbon deposition can also rapidly decrease cell performance and even cause irreversible

cell damage.[19–21] For instance, when fueling SOFCs directly with carbonaceous fuels, such as biogas,[22] natural gas,[23] syngas,[24] or diesel reformat,[25] the risk of carbon deposition is very high. As an example, when operating an SOFC stack with a fuel mixture that contains 39.6% H$_2$, 11.91% CH$_4$, 25.67% H$_2$O and 22.78% N$_2$ for 800 h at an operating temperature of 750 °C, strong amounts of degradation were observed during the initial 300 h of operation.[26] During the subsequent 500 operating hours, stable operation but also significantly reduced cell performance were observed. The authors of this study measured a degradation rate of approximately 1.42%. This degradation was mainly due to the deposition of carbon in the form of carbon nanofibers. For anode-supported SOFCs that were operated under methane with an S/C of 0.5 at 800 °C, rapid performance deterioration and microstructure degradation were observed.[15] Moreover, in another study, the authors claimed that increasing the amount of CH$_4$ in a simulated syngas resulted in strong amounts of performance degradation and even irreversible morphological degradation, particularly when the amount of methane exceeded 23%.[27] Operation under dry methane at 800 °C resulted in the abundant growth of whisker-type carbon filaments, which impacted the Ni catalysts and the anode porosity.[28] A detailed numerical study on SOFCs operated under methane with varying S/C ratios indicated that, when in equilibrium state, 0.5 mol of graphite is formed from 1 mol CH$_4$ at 700 °C, and 0.6 mol carbon-nanofibers is formed at 750 °C.[29] Equimolar mixtures of CO and CH$_4$ showed similar results. Many studies have been carried out to scrutinize the phenomenon of carbon deposition under open-circuit voltage (OCV) conditions, showing that carbon deposition has strong impact on the cell performance and its microstructure.[30–34] However, in order to investigate the impact of the operating environment on the systems for application in real-life scenarios, it is crucially important to examine the operation under load conditions. In general, all degradation effects begin with the Ni catalyst, although different impurities cause performance deterioration. Mechanisms that influence Ni morphology include: (i) Ni reoxidation, (ii) Ni agglomeration, (iii) Ostwald ripening, (iv) Ni deposition on the ion-conducting grains within the anode and (v) Ni deposition on the electrolyte surface.[35] Additional degradation occurs due to thermal expansion mismatch. If all of the aspects mentioned previously are considered, we can conclude that SOFC durability can be impacted by: (i) intrinsic degradation mechanisms, which are initiated by operating conditions, such as high-operating temperatures or operating currents, and (ii) extrinsic degradation mechanisms, which occur as a result of fuel impurities.[35]

Although a basic understanding of failure modes and damage phenomena exists, the entire SOFC industry is still facing a significant problem, because there is yet not enough information about the degradation behavior of stationary power generators over long lifetimes (>40 000 h). It would be possible to obtain this information if systematic damage analyses were carried out. This information would enable degradation to be identified in its preliminary stage and even allow it to be reduced. Another problem is the fact that validation tests run for 40–80 000 h would take many years to carry out, so

procedures must be developed that allow researchers to demonstrate the durability of these systems in accelerated tests. To achieve this purpose, the operating conditions were adjusted in the present study to accelerate a specific degradation mechanism that is relevant for a real-system application, namely, carbon deposition-based SOFC degradation. These investigations were performed under operating conditions that are relevant for industrial application; thus, the system operation under load conditions using methane as fuel and SOFCs of industry-relevant dimensions were considered. This enabled us to obtain highly detailed insights into the degradation processes that occur during the cell operation and determine how this degradation could be identified early on. Next, we addressed two specific challenges: (i) to improve the system reliability and durability and (ii) to develop tools that allow us to identify different failure modes at a preliminary stage. *In situ* near-IR thermal imaging was identified as an appropriate tool to investigate the behavior of the button-cell anode when using carbon-containing fuels (*e.g.* humidified ethanol and direct fuel oxidation), as well as potentially damaging processes.[36,37] Thermal imaging has also already been used to characterize the operation of high temperature electrolysis.[38] Moreover, the method of *in situ* vibrational Raman spectroscopy has also been used successfully to identify both rates of carbon depositions[32,39,40] and its removal from the Ni/YSZ anodes.[32] Applying the *in situ* Raman spectroscopy, the authors[32] showed that H_2O, CO_2 and O_2 can be employed to remove the carbon formed, but also that the carbon removal has to be performed carefully to prevent undesired Ni reoxidation. By applying unconventional online monitoring tools based on the total harmonic distortion (THD) principle, it seems possible to identify cell degradation at its preliminary stage, before irreversible degradation occurs. In addition, the integration of these online monitoring tools into the running systems can be easily accomplished. To date, fuel cells under operation have mainly been monitored online by applying conventional tools, such as polarization curve or the more sophisticated electrochemical impedance spectroscopy.[41–44] When employing electrochemical impedance spectroscopy, a linear and time-invariant system state is assumed. The information obtained by taking EIS measurements provides more detailed insights into the process mechanisms occurring inside the cells. Recently, EIS data recorded could be used in a distribution of relaxation times analysis (DRT) to observe the time constants of individual processes.[45–49] By employing the DRT analysis, researchers could identify the electrochemical properties of microtubular ASC-SOFCs as a function of their microstructure.[50]

However, if the criterion of system linearity is neglected, undesired processes within cells are assumed to occur. These can be identified when employing an *in situ* total harmonic distortion analysis method. This methodology has already been employed in the field of electrical engineering to reduce nonlinear loads in power sources. Its potential has also been successfully demonstrated in low-temperature cells,[51–53] increasing the understanding of the effects of fuel and oxygen starvation. The same effects, which are related to fuel and oxygen starvation, were recently reported for anode-supported

SOFCs, consisting of Ni-YSZ/YSZ/LSCF.[15] In another study that dealt with application of THD for SOFC,[54] fuel starvation was investigated on the stack level, and the THD results were higher than 1% when fuel starvation occurred. Moreover, the nonlinear impedance approach was taken to identify distinctive aspects of electrochemical mechanisms occurring at the LSCF electrode at 750 °C, which could not be observed in linear EIS.[55]

Since the electrolyte-supported Ni-GDC/ScSZ/LSM SOFCs used in this study are intended for use as a core of an auxiliary power unit, which is operated with natural gas with an integrated desulfurization system, the most critical degradation processes based on carbon deposition are investigated and presented in this paper. The cells were operated under load conditions, as in the real operating case. It was possible to identify carbon that formed on the SOFC anode rapidly and early on by applying the THD methodology. Thus, in this paper we present a method that can be used to identify SOFC degradation early on, as well as a strategy that can be applied for efficient carbon removal and performance regeneration. The findings of this study improved the understanding of (i) the operation of and processes that occur within industrial-sized electrolyte-supported solid oxide fuel cells (ESC-SOFCs) that have been designed to be used in an auxiliary power units (APUs) and operated directly with methane, (ii) the application of unconventional online-monitoring tools, based on the THD principle, which can be used to identify undesired degradation and carbon removal mechanisms, and (iii) strategies for carbon removal that allow us to re-attain the initial cell performance, as observed in the degradation-free state.

2 Experimental setup and methods

The experimental investigations were carried out on electrolyte-supported (ESC) single-cells that were manufactured by the Fraunhofer Institute IKTS. The cells had an average thickness of 0.17 mm. The fuel electrode was screen-printed nickel–oxide with fully gadolinia (Gd_2O_3) stabilized ceria (CeO_2) on the 10ScSZ electrolyte, whereby the oxygen electrode consisted of co-doped lanthanum strontium manganite ($La_{1-x}Sr_xMn_{1-y}M'_yO_{3-\delta}$). The overall area of the single-cells was 10 cm × 10 cm with an electrochemically active area of 81 cm^2. For more detailed information about the microstructure and materials of the cells used we refer to other studies.[56,57] For the purpose of experimental investigations, the cells were embedded in a ceramic-cell housing.

The gas inlet and outlet pipes were manufactured as alumina and heated up to the operating temperature in an electrical furnace. Glass sealing was used to prevent gas from leaking between the electrodes. On the fuel electrode, Ni meshes were used as contact point. On the oxygen electrode, a platinum mesh was used. No contact pastes were used. The temperature was measured at six different points on the fuel electrode, six points on the oxygen electrode, and on both the fuel and air inlets and outlets. A mechanical load was applied to decrease the contact resistance. For more detailed information about the test rig and ceramic housing used (Fig. 1), as well as their
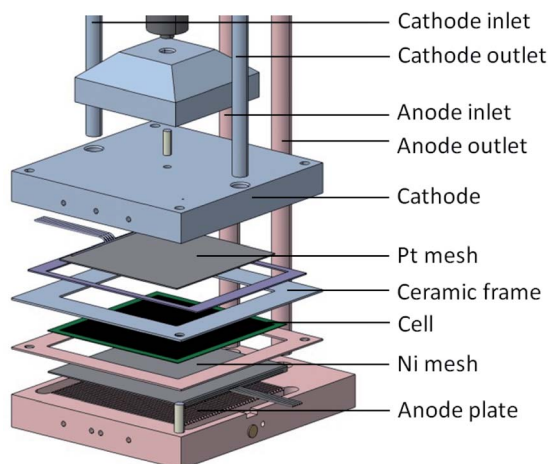
Fig. 1 Ceramic cell housing.[59]

impacts on the measurements, we refer the readers to previous studies.[58,59]

The operating temperature was set at 800 °C. Since the SOFCs used should be employed as a part of a system, lower operating temperatures are preferred. Both hydrogen and methane were used as fuels, while the cathode was supplied with synthetic air. A mixture of hydrogen and nitrogen was used to initially characterize the cell performance, whereby methane was used to induce cell degradation based on carbon deposition. The methane fuel was humidifed using a humidifier unit based on the bubbler principle. The S/C ratio was varied between 1 and 0.5. In order to accelerate the cell degradation, the S/C-ratio was set to 0.5. Considering the outcome of a numerical study on the probability that carbon is formed as a function of operating temperatures, it was shown that when using methane with S/C = 0.5 as fuel, the amount of carbon nanofibers formed is highest between 700 °C and 800 °C, while it decreases as the temperature increases. Moreover, to conduct long-term investigations, the operating current was set at 50 mA cm^{-2}. This decision was made to accelerate carbon depositions, since a higher amount of carbon deposition was expected at lower operating currents. Nevertheless, all the electrochemical processes occur under the current density selected. Subsequently, the hydrogen/steam mixture was used as a regeneration mixture to remove carbon and achieve an initial cell performance; thus, the cell performance was considered before the degradation occurred. The parameters applied in the experimental investigations in this study, in which the fuel gas composition, fuel and air volume flow and operating temperature were considered, are shown in Table 1. Throughout the study, we continuously analyzed the inlet and outlet fuel gas with an ABB gas analyzer with a measurement uncertainty <1%. Five cells were used to ensure the reproducibility of the results. The maximum performance deviation observed for different cells over the entire load range (the lowest operating voltage of 0.7 V) was ±3%. According to these observations, slight oscillations in the AC measurements occurred. However, the specific frequency ranges remained unchanged.

To perform the electrochemical analysis, measurements of polarization curves and electrochemical impedance spectroscopy (EIS) were made employing a Gamry reference 3000 potentionstat/galvanostat with an appropriate booster. The measurement uncertainty for the DC range accounted ±0.3%, while for the AC range the accuracy was higher than 99%. In addition, a total harmonic distortion analysis was performed with subsequent post-processing of the data measured as a primary tool to identify degradation at its earliest stage. The initial EIS and THD characterizations were performed over the entire load range; specifically, the operating current was increased while the voltage was simultaneously decreasing down to 0.7 V. The sine current was superimposed with an amplitude 4% of the DC value. The voltage response was measured. Moreover, the measurements were performed in a frequency range of 20 kHz to 10 mHz. The measurements always began with the higher frequencies and proceeded toward the lower frequencies. The measurement procedures for electrochemical impedance spectroscopy and total harmonic distortion analysis are, in principle, very similar, but the subsequent data evaluation methods differ. While the EIS assumes system linearity, the THD is observed for non-linear systems. In a linear system, the signal distortion from the fundamental oscillation is very low, and the THD approaches zero. The THD data are generated by applying the fast Fourier transformation (FFT), during which the signal measured is converted from its original time domain to the frequency domain. Here, total harmonic distortion presents a ratio between two relevant signal response amplitudes: this is a sum of all higher harmonic frequencies and the fundamental frequency. For the purpose of this study the current was controlled and maintained at a constant level, allowing the voltage response to be measured. Therefore, signal distortions observed in this study are related to the measured voltage response. Taking this into consideration, the THD shown

Table 1 Operating parameters used

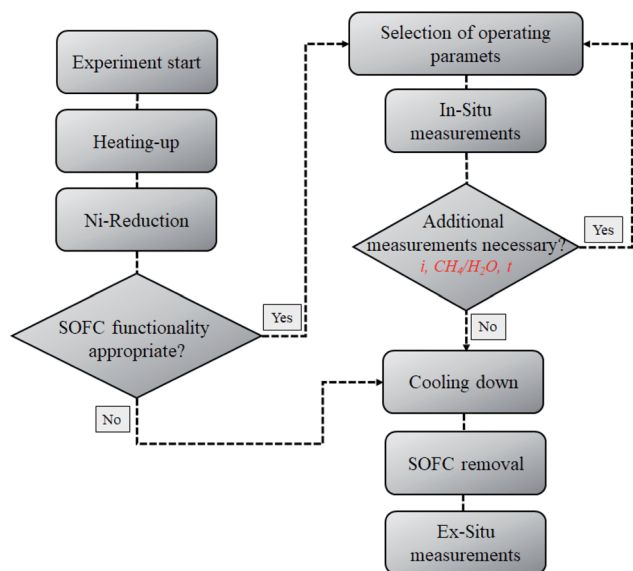| Operating parameters, units | Fuel electrode | | | | | | | Oxygen electrode | | |
	ϑ, °C	i, mA cm^{-2}	x_{CH_4}, %	x_{H_2}, %	x_{H_2O}, %	x_{N_2}, %	$\dot{V}_F$, SLPM	x_{O_2}, %	x_{N_2}, %	$\dot{V}_O$, SLPM
Fuel mixture F20	800	50	20	0	20	60	2.4	21	79	1.9
Fuel mixture F40	800	50	40	0	20	40	2.4	21	79	1.9
Regeneration mixture RM	800	50	0	40	20	40	2.4	21	79	1.9

Paper

Fig. 2 Simplified flow chart for the experimental investigations performed.

reflects the system non-linear behavior and enables us to quantify the non-linear signal distortion.

Finally, microscopic investigations of the anode surface were carried out. A Zeiss Ultra 55 field emission scanning electron microscope (FE-SEM) was used to investigate the anode microstructure. It was not necessary to coat the cell surface and, thus, the cell analysis was unobstructed. A simplified flow chart of the experimental procedure applied is shown in Fig. 2.

3 Results and discussion

The results obtained from the SOFC stability and durability tests are presented in this section, placing a main focus on the (i) carbon deposition failure mode and the (ii) carbon removal, performed to re-attain the initial cell performance. Comprehensive electrochemical, temperature, gas and post-mortem analyses were performed. In some cases, traditional methods (polarization curves, electrochemical impedance spectroscopy) that were used to characterize cell performance do not allow to reproduce the real states in the cells and, in fact, do not enable important information (*e.g.* formation of carbon) to be collected, as we discuss below. By applying non-conventional tools based on the THD principle, it was possible to gain more detailed insights into cell performance and the internal cell environment. To improve the accuracy of the THD methodology used, the carbon deposition degradation was induced in a controlled manner. After ascertaining that the expected degradation mechanisms had occurred, a customized cell regeneration strategy was employed to remove the contaminants from the anode surface and regain the initial performance.

3.1 Identifying degradation

The initial SOFC reliability under operating conditions with carbon-containing fuels was examined by fueling the anode directly with a methane/steam mixture (S/C of 1) at an operating temperature of 800 °C. Thus, the effects of internal methane steam reforming and its impact on the cell performance were examined in detail. At the same time, the cathode side was supplied with synthetic air. Detailed information about the operating conditions can be found in Table 1. *In situ* performance monitoring indicated that the SOFC performed stably and continuously, and no visible changes were observed. A gas analysis was performed, and the results showed a continuous methane conversion rate. Electrochemical impedance spectroscopy indicated constant losses over time. Voltage monitoring data collected also indicated stable operation. During the approximately 20 h of operation under methane and the applied current density of 50 mA cm^{-2}, no voltage oscillations were observed. A low current density was set in order to accelerate carbon formation. To further accelerate performance alteration and induce degradation based on carbon deposition, the S/C ratio was decreased down to 0.5; the cell was then operated under these conditions for 90 h.
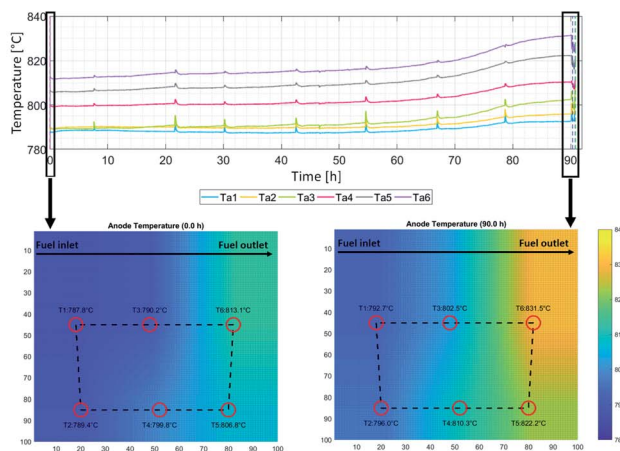
An analysis of data obtained while fueling the cell with methane was conducted. In this investigation, a S/C of 0.5 was used, and the operating temperature was maintained at 800 °C. When applying conventional methodologies, such as voltage monitoring, we assumed that the SOFC operation under
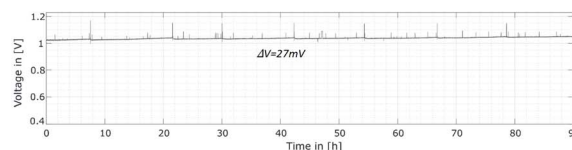
(a) Voltage monitoring.
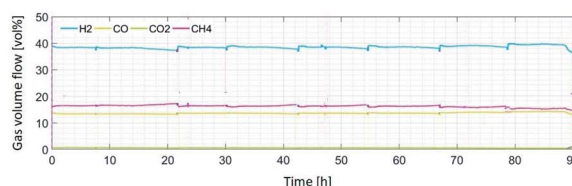
(b) Gas analysis during the cell operation.

(c) Temperature distribution over the anode surface.

Fig. 3 Performance monitoring for the S/C-ratio = 0.5.

methane would be stable during the 90 h period, as illustrated in Fig. 3a. During this period, a very slight increase in voltage as a function of time was observed. Such an increase may even indicate a slight improvement in performance. Formation of a local thin carbon layer can also improve the cell performance over brief periods. Linking carbon particles and the nickel catalyst sites together, without decreasing the anode porosity and thus inhibiting the gas distribution, improves the electrical cell conductivity and can result in an increase in the voltage measured. The performance enhancement resulting from the formation of carbon deposits was initially reported for Cu-ceria-YSZ anodes[60] and confirmed afterward by other studies.[61,62] However, additional analyses need to be carried out to obtain more precise information about the cell performance. When considering other measured parameters, such as the temperature distribution, an overall temperature increase of approximately 10 °C was observed during the last 25 h of operation, as shown in Fig. 3c. This temperature increase may indicate the presence of different, undesired degradation mechanisms within the cell, such as (i) carbon depositions which can inhibit further CH_4 reforming, or (ii) enhanced CH_4 oxidation and H_2 oxidation, both of which result in an increasing temperature. Moreover, such mechanisms can influence increases in the area specific resistance (ASR), which, in turn, leads to temperature increases. Considering the overall cell surface and 2D temperature distribution (see Fig. 3c), the strongest increase is observable on the anode outlet side. To interpret such alterations properly, further analyses must be carried out, such as gas analyses and post-mortem analyses.

Initially, the equilibrium calculations were performed showing the following gas composition: 48.9 vol% H_2, 1.8 vol% CH_4, 0.2 vol% CO_2, 9.3 vol% CO, 0.95 vol% H_2O and the remaining N_2. The equilibrium calculations reveal slight deviations from the measured gas compositions, which originate from slight leakages in the experimental setup as well as reaction kinetics and electrochemical reactions that are not considered for thermodynamic equilibrium calculations. Next, it is very important to consider that GDC in the anode electrode is specifically designed to prevent CH_4 cracking and carbon depositions but also to enhance steam reforming. This is revealed by the higher measured volume fraction of CH_4 and lower measured volume fraction of H_2. Considering the S/C ratio of 0.5 and the initial CH_4 volume fraction of 40 vol%, it can be assumed that 20 vol% CH_4 could be converted completely by steam reforming. The remaining converted CH_4, which accounts approximately 4 vol%, may be converted by dry reforming or methane cracking processes. As the operating time increases, this ratio changed slightly and more carbon was formed.

The results of the gas analysis (see Fig. 3b) carried out during the entire operating time show a slight decrease in the methane fraction measured at the anode outlet as a function of operating time. Initially, a 16.5 vol% of CH_4 was measured. After 85 h, this fraction had dropped down to 15.1 vol%. At the same time, the H_2 and CO fraction increased. The initial volume fraction of H_2 was measured as 38.4 vol%, whereby it had slightly increased up to 38.8 vol% after 85 h of operation. The CO quantity remained constant during the initial 20 h, but rose during the last 20 h (from 13.4 vol% up to 14.3 vol%); this correlated with a decrease in CO_2. Such an effect could be linked to the more pronounced dry-reforming process that occurred during this time. In one study,[63] an increased quantity of H_2 generation did not correlate with an increase in CO, but could be associated with the CH_4 decomposition. Moreover, when examining unsupported Ni catalysts, another study reported that increasing the CH_4 decomposition rate resulted in carbon depositions.[64] Thus, more CO_2 was consumed and the quantity of CO produced was higher than predicted, since the equilibrium of the Boudouard reaction was shifted.

Regarding the steam- and dry-reforming processes, these are endothermic reactions. The effect of the endothermic reaction was especially visible on the anode inlet side, at which the temperature decreased by 13 °C as compared to the furnace-controlled temperature of 800 °C; this temperature was 27 °C lower than the temperature on the anode outlet side. During the initial 30 h of operation, the temperature decreased at the anode inlet, indicating that enhanced reforming was occurring in this specific area as a function of time. As the operating time increased, the temperature increase could be observed over the entire cell surface. The temperature and gas analysis results thus provided additional information about possible chemical and electrochemical reactions that occurred in the cell. To obtain more detailed insights into the SOFC performance, electrochemical studies based on electrochemical impedance spectroscopy and a total harmonic distortion analysis were performed.

Fig. 4a shows the Nyquist plots for the frequency range between 15 kHZ and 10 mHz, observed over the operating time of 90 h. In this figure, the measurements at the specific time points of 10 h, 40 h, 50 h, 60 h and 90 h are presented. Slight instability was clearly observed at the lowest frequencies. This occurs due to the high steam content and the ongoing slow reactions, which continuously and slightly varied the concentration of specific fuel components. For this reason, such deviations had to be identified in the system, and a specific threshold value had to be determined. This enables to illustrate the correct cell behavior and avoid interpreting slight changes as false degradation.

A more detailed explanation is provided below. Moreover, in Fig. 4, the alteration of the impedance magnitude (Fig. 4b) as well as the measured response distortion (Fig. 4c) are presented along the y-axis. The x-axis shows the timeline of the experiment, which was 90 h overall. The color scale indicates the intensity of the changes that occurred during the operation, which were up to 0.01 mΩ cm². When considering the magnitude alteration, as can be seen in Fig. 4b, the most pronounced alterations with an intensity of 0.01 mΩ cm² are visible at very low frequencies, lower than 1 Hz, and these occur in constant intervals of approximately 10 h. These alterations correlate with the refilling of the humidifier system, which can disturb the fuel equilibrium over short periods, since a slight temperature change initially occurs. The THD response (approx. 5%) can also be observed at the same time points, as shown in Fig. 4c. At higher frequencies, a stable operation without any
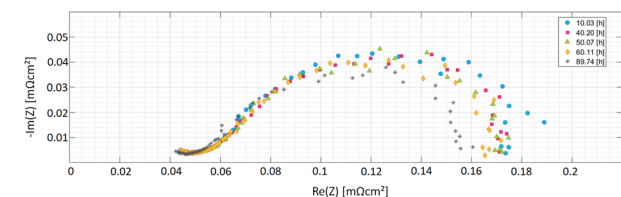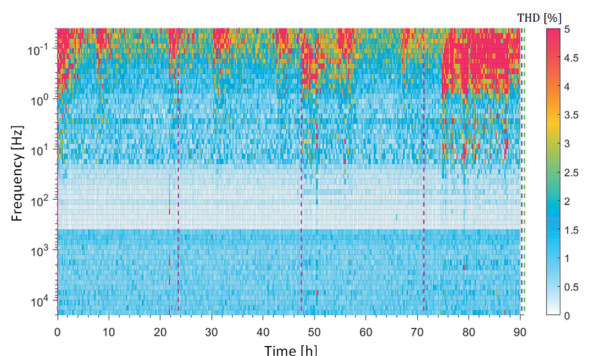
(a) Nyquist plots as a function of the operating time.
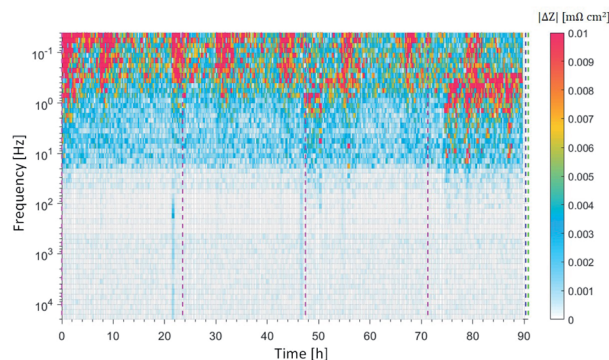
(b) 2D impedance distribution

(c) 2D THD distribution

Fig. 4 THD monitoring during the operating time of 90 h.

significant changes or distortions was observed. The distorted signals are, however, clearly visible in the frequency range between 10 and 0.1 Hz. We surmised that this distortion arose from changes induced by carbon formation within the anode channels and the catalyst. The hypothesis was supported by the results of microscopic investigations, which are illustrated in Fig. 6. The carbon was mainly deposited in the form of carbon nanofibers which covered much of the anode surface (see Fig. 6a and b). However, the greatest amount of carbon was found at the anode outlet; this can be seen in the picture of the anode after its removal from the cell housing, as shown in Fig. 6d. It has to be mentioned here that the cell was mechanically damaged during its removal from the ceramic cell housing and, more precisely, during its separation from the ceramic frame to which it was connected using a glass seal. Although carbon was deposited over the entire anode surface and even caused slight alterations in the anode microstructure, the electrochemical reactions were not inhibited by this deposition, since the porosity sufficiently enabled undisturbed

gas diffusion, and the catalytic active sites remained available. For this reason, no voltage decrease was determined, and the power generated remained constant.

These findings enable us to reach two important conclusions: (i) the preliminary stage of degradation cannot be observed with conventional online-monitoring tools, indicating that the irreversible degradation stage can easily be reached without prior detection, and (ii) the present cell type is highly resilient towards carbon deposition; although carbon depositions formed, and surface changes occurred, the cells could be further operated without an observable reduction in the power generated. Although the SOFC performance was not strongly affected by carbon deposition in the present study, we observed massive carbon deposits in the anode outlet lines, as shown in Fig. 6d. These may have been due to the increase in temperature that occurred at the anode outlet. Carbon accumulates in the pipe and, after a specific length of time, this carbon can inhibit the removal of the exhaust gas, causing an undesired system shut-down. The carbon that accumulated in the anode outlet pipe was analyzed post-mortem, and the image taken is shown in Fig. 6c.

More detailed insight into THD response of the individual frequencies is obtained when separating the frequencies into specific ranges, as presented in Fig. 5. The average THD value over a frequency range is shown for the following: (1) 0.04–2.50 Hz (indicated by red color), (2) 2.50–31.25 Hz (indicated by black color), (3) 21.25–398 Hz (indicated by blue color), and (4)
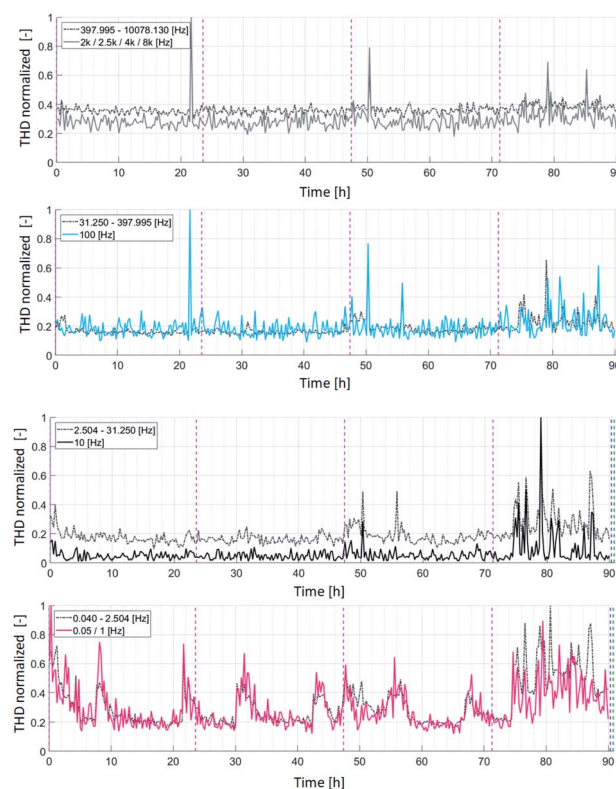

Fig. 5 THD monitoring of individual frequencies during the operating time of 90 h.

398–10 078.13 Hz (indicated by gray color). For each of the frequency ranges mentioned, the cell behavior under the specific selected frequencies is presented in addition, thus taking into account the following frequencies: 0.5/1 Hz, 10 Hz, 100 Hz, and 2/2.5/4/8 kHz. This behavioral analysis was carried out to determine the range of frequencies at which the carbon deposition phenomenon is predominantly visible. The operation time is presented along the x-axis, whereby the y-axis shows the THD normalized with regard to the maximum values over the entire frequency range. Thus, it seemed to be simpler to present the significance of the individual peaks observed.

Almost no changes were detected during the 70 h of SOFC operation with methane at frequencies higher than 30 Hz. Two very high peaks were observed after approximately 21 h and 50 h. The peak observed after 21 h was observed only in the frequency range from 30 Hz to 10 kHz, but not at lower frequencies. We assume that this peak results from fast processes, as oscillations only occurred briefly around the equilibrium state. The peak occurrence seemed to be influenced by the fuel mixture used and the high steam quantity in this mixture.

For frequencies ranging from 0.04 to 2.5 Hz, the THD signals were observed periodically at 10 h intervals. These signals correlate with the humidifier system, as already stated above. Based on these results, the changes that occurred in the inlet fuel could be identified by distortions at 0.05 Hz. Very strong distortions were observed for the first time after 50 h, throughout the entire frequency range, but more specifically for the following frequencies: 0.05 Hz, 10 Hz, 100 Hz, 2 kHz, 2.5 kHz, 4 kHz and 8 kHz. After these oscillations were observed, the initial state was regained. Afterward, signal distortions were observed after approximately 75 h throughout the entire frequency range, which indicates that carbon deposition impacts not only the mass-transfer processes, but also contacting and the overall cell conductivity.

Distorted impedance was most pronounced in the low frequency range, $i.e.$, for frequencies below 30 Hz. However, distortions were also clearly visible at higher frequencies, which is highly advantageous in terms of the measurement time. In such cases, all information required can be obtained when performing measurements at higher frequencies ($i.e.$ 2 kHz, 2.5 kHz, 4 kHz and 8 kHz), enabling the measurements to be carried out over short period. This also enabled the identification of degradation at an early stage. However, if different degradation mechanisms are expected to occur simultaneously in the system, it is first necessary to exclude the possibility that different processes provide the exact same specific high frequencies.

Moreover, a low level of distortion (approximately 2%) was determined at the beginning of the investigation, which was identified as a threshold value. This distortion stemmed from the fuel mixture used and the processes that occur, which have an impact in the form of continuous slight oscillations around the equilibrium state. When comparing the results obtained in this study with those from other available studies, it is important to note that THD has been used in only a limited number of studies to analyze several failure modes, most of which are studies on low-temperature fuel cells.
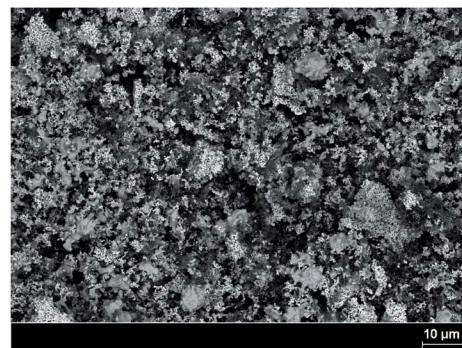
(a) Carbon observed at the anode outlet.
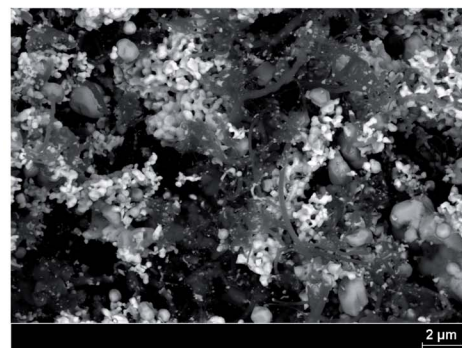
(b) Detailed view of the anode surface.
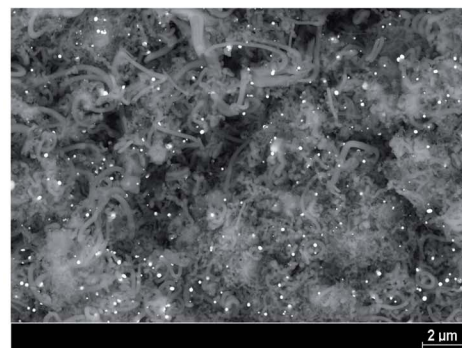
(c) Carbon in the anode outlet pipe.

(d) Anode outlet pipe and anode after experiment.

Fig. 6 Pictures and SEM images taken after 90 h operation with humidified methane at an S/C of 0.5.

THD has already been successfully employed for PEM to compare Damjanovic ORR mechanisms with oxygen electrochemisorption and oxygen chemisorption mechanisms.[53]

Moreover, another research group used THD to obtain more information about mass-transfer losses related to fuel and oxidant starvation in PEM cells.[52] For this purpose, they restricted the amplitude used above 1% and below 5% of the DC load applied. Regarding the oxidant starvation, the harmonics significantly decreased as the frequency increased and were visible mainly at frequencies below 100 Hz. In contrast, the fuel, or namely, hydrogen starvation was observed only at frequencies below 15 Hz. The same effects were investigated for anode-supported SOFCs,[15] but these cells are manufactured using processes and materials that significantly differ from those used to fabricate the ESC-SOFCs used in the present study. With respect to both effects, signal distortion could be observed at frequencies below 10 Hz. At higher frequencies, the impedance was undistorted. The carbon deposition phenomenon could be identified at similar frequency ranges, indicating that the THD methodology could be used to identify the specific failure mode.

The data visualization method used, which is more appropriate for practical applications, is shown in Fig. 7. The first indication that changes had occurred was observed after approximately 50 h of operation, as already discussed above. The mean value of distortion had not reached a maximum by that time point. After operation was continued without taking any appropriate actions to counteract this effect, and the cell was operated for another 40 h. However, beginning at 80 h, very strong THD signals appeared. These did not disappear even after another 10 h; instead, they intensified. These signals indicated that irreversible changes had occurred in the system under operation and resulted in its eventual shutdown.

The appropriate measurement procedures must be employed to identify the relevant outliers and to process the information they provide. Therefore, the quality and linearity of the measured data must be determined early on, *i.e.*, at the beginning of the experiment. If the outliers are ignored and considered as indicators of the extraneous, poor quality of the measured data, the system under operation could be destroyed rapidly after being operated for a specific period. In the case shown, no appropriate actions were taken after 50 h, but the cell was operated still further, until an irreversible degradation state was achieved. However, if suitable countermeasures are taken when only a slight degradation has occurred, which can be identified by the presence of outliers (*i.e.*, as observed in our study after 50 operating hours), the overall system lifetime can be significantly prolonged.

3.2 Carbon removal and performance regeneration

In order to prolong the undisturbed system operation period, further tests were performed. The already defined operating conditions were established to initiate carbon deposition after approximately 50 h of operation and to apply appropriate carbon removal strategies. Initially, different fuel mixtures were used to compare the impacts of different fuels on the measuring signal quality, as indicated by the height of THD signal, and to determine the threshold value for different fuels. The fuel mixtures were supplied to the cell as follows: $H_2/N_2 = 40/60$, $H_2/H_2O/N_2 = 40/20/40$ and $CH_4/H_2O = 40/20$. Their impacts on the signal distortion are shown in Fig. 8. No distortions could be observed when fueling the cell with dry hydrogen. When the fuel was switched to humidified hydrogen, slight distortions of approximately 1% were identified. Moreover, feeding the anode with humidified methane resulted in higher levels of distortion.
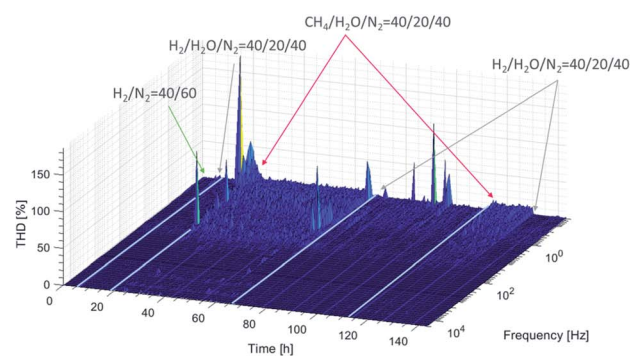
(a) 3D THD analysis results.
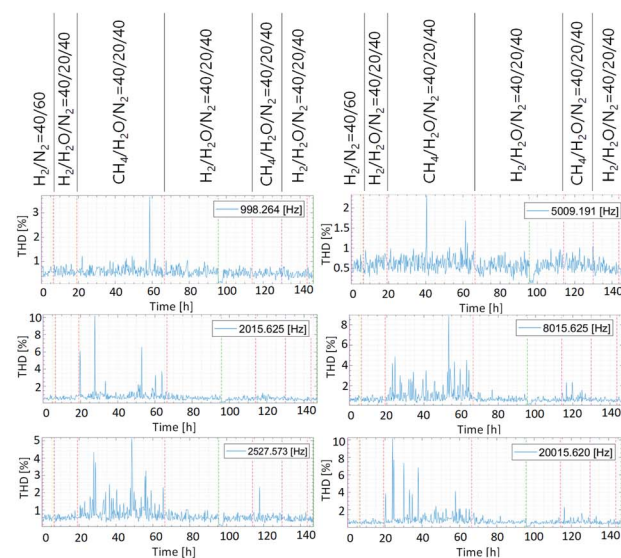
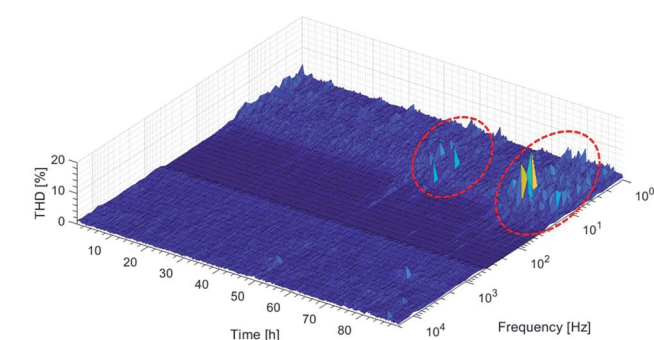

(b) Individual frequencies for the SOFC operation.

Fig. 8 Identification of SOFC degradation and regeneration processes.

Fig. 7 THD monitoring of SOFC performance and degradation during the operating time of 90 h.

This distortion is induced by variety of chemical reactions that occur and the oscillations around the equilibrium state.

Very high THDs were observed at the initial point in the investigation, when the fuel was changed to methane, until the equilibrium state was reached. After the equilibrium state was reached, the THD threshold was identified as approximately 2.5%. An increase in the THD value thus indicates that specific changes have taken place in the operating system. The cell was operated for 50 h with humidified methane, after which the first THD signals were observed, as expected based on the results of the previous experiments performed. These indicate that carbon was deposited on the anode surface and that it needs to be removed.

In order to remove carbon, we applied a regeneration mixture that contained hydrogen and steam. This regeneration mixture was effective and highly time-efficient in this case, since the carbon deposition process was still at its preliminary stage. Its effectiveness has already been proven and described in previous works.[58,61] In those studies, carbon depositions could be completely removed and the initial cell performance could be regained in anode-supported SOFCs by feeding them with humidified hydrogen. Since the anode thickness is significantly lower in the electrolyte-supported SOFCs used in this study, and because the mixed ionic/electronic conductor used had a lower propensity to deposit carbon, the overall regeneration time required could also be reduced.

During the carbon removal procedure, several individual peaks were observed, and especially peaks in the low frequency range. We concluded that these indicated the point at which the carbon deposits are first removed from the anode surface; these first appeared after 10 h. Afterward, high peaks with an increased intensity are seen after 20 h of fueling with the regeneration mixture. These peaks could be detected for several hours. It seems as though complete removal of the deposits was achieved during this period, and the initial performance was regained. After the regeneration procedure had been completed and determined as successful, the fuel mixture was switched to the humidified methane to validate the cell performance. Operation under methane took about 10 h, and stable performance was monitored that was equal to the initial performance achieved. Subsequently, the H_2/H_2O-mixture was used, and no performance alterations were observed, indicating that a degradation-free state existed inside the cell.

More detailed information about the individual frequencies observed during fueling with different mixtures, which are indicative of the reference cell performance, degradation, and regeneration processes, is provided in Fig. 8b. The analysis was performed for the frequencies of 1 kHz, 2 kHz, 2.5 kHz, 5 kHz, 8 kHz and 20 kHz to decrease the overall measuring time. Employing a H_2/N_2 mixture as a fuel resulted in the observation of almost no distortions. This finding was expected, since the equilibrium state can be reached almost immediately and very stable operation is expected to occur when using dry hydrogen. Moreover, no possible degradation mechanisms can occur, except for a slight amount of material degradation that arises as a function of operation time after several thousands of hours. The signal distortions slightly increased when humidified

hydrogen was used, but this difference can almost be neglected. If the H_2/H_2O-ratio is sufficiently high, no degradation is expected to occur. Nevertheless, if the steam quantity in the fuel mixture is very high and much higher than hydrogen quantity, Ni reoxidation processes can occur, which can even cause irreversible morphological changes. In the present study, the H_2/H_2O-ratio was maintained at two, which ensured safe SOFC operation and prevented any undesired degradation. Next, the basic level of signal distortion observed at approximately 2.5% was much higher for the CH_4/H_2O mixture than for any of the other fuel mixtures. Especially high values were observed at the initial cell state at the following frequencies: 2 kHz, 2.5 kHz and 20 kHz. This indicated that the equilibrium state existed at each of these frequencies. After approximately 50 h, clear signs of carbon formation were detected. Considering the specific frequencies shown, all of these indicated that carbon deposition had occurred. However, the signal amplitude and the signal incidences differed at different frequencies. At 2.5 kHz, the THD had a value of approximately 3%, which increased up to 5–10% at 8 kHz. Once these appeared, the THDs were observable for 15 h. At 1 kHz, only one peak was detected after 40 h of operation, with a distortion of 4%. For the frequency of 2 kHz, three distortions were recorded altogether between 35 and 50 h of operation. The first one had a value of 6%, and the remaining two had values of approximately 4%. Slight distortions were observed for the remaining frequencies, with 1.5% measured at 5 kHz after 45 operating hours and 4% measured at 20 kHz after 40 h. Regarding the carbon removal, no clear indication of carbon removal and its identification could be observed for the specific selected frequencies. This is more clearly visible at lower frequencies in Fig. 8, which also resulted in an increase in measurement time. When the fuel used was changed from humidified hydrogen to methane, slight distortions were observed at 2.5 kHz, 8 kHz and 20 kHz, which are associated with the time required to reach an equilibrium state. Afterwards, a stable continuous operation was observed.

4 Conclusion

This work moves away from the conventional methods of characterizing SOFCs towards the application of novel online-monitoring tools to identify degradation mechanisms in their preliminary stages. The results indicate that this application is a highly effective approach that can be taken to determine whether undesired processes are taking place within cell that cause alterations from the steady state. The relevant critical conditions identified when operating SOFCs under real-life application scenarios and, namely, carbon deposition due to a low S/C ratio, were examined by applying THD. The S/C ratio of 0.5 was utilized in this study, which caused irreversible morphological degradation over a period of 90 h. Rapid degradation occurred due to the extremely low S/C-ratio and low operating current density of 50 mA cm^{-2}, which were selected to accelerate the degradation processes. By applying a non-conventional THD tool, we could rapidly identify the failure mode examined. Frequencies of 2 kHz, 2.5 kHz, 4 kHz and 8 kHz were identified as relevant for carbon deposition identification.

Since the frequencies are in the third order of magnitude, the measuring time required is thus low. Employing conventional electrochemical impedance spectroscopy when fueling SOFC with methane requires the measurements to be performed until very low frequency of 10 mHz. Based on the frequency range necessary and depending on the measurement setting, one measurement can take more than 20 minutes. In contrast, when employing the THD methodology presented in this study, the measurements have to be performed only at specific relevant frequencies, thus reducing the overall measuring time at most several minutes and, in specific cases, by a factor of 15–20. This significantly simplifies the measuring procedure. Appropriate mitigation strategies and regeneration approaches can be used to prolong the system lifetime only if the degradation is identified at its preliminary and reversible stage.

The power generated from the SOFCs used remained almost unchanged even after 90 h of operation, and the electrochemical processes continued. Thus, the cells displayed a stable performance and strong durability; this indicates that they may serve as the first choice for further commercial applications. The signal amplitude of 4% was identified as appropriate to identify higher harmonics that occur if the cell moves out of the safe operation state and if undesired degradation processes and contaminations occur in the running system.

Moreover, we verified that this served as an effective method to regenerate cell. Using this method, if carbon deposition is identified at an early stage and is removed by applying already proven regeneration strategies, the initial cell performance can be effectively regained. However, carbon removal processes could not be identified at higher frequencies, but only at lower frequencies, indicating that longer measurement period are needed for these processes than were required to identify whether carbon deposition had occurred. The methodology applied in this study is crucially important in that it allows a state-of-the-health analysis to be made and, thus, predictions to be made regarding the remaining SOFC lifetime. This methodology also can be used as a low-cost, online-monitoring and diagnostic tool for commercial SOFC systems. The study has been carried out on the industrial-sized cell level to examine the most relevant degradation phenomenon that can occur in real system under operation with natural gas: carbon deposition. A further step is validation of the approach on the stacks level and analysis of diverse degradation modes. This is also a requirement for very efficient separation between different degradation mechanisms that occur simultaneously, in order to identify the overlapping frequencies and separate only singular process-specific frequencies for further application.

Author contributions

Vanja Subotić – conceptualization, methodology, validation, investigation, visualization, data curation, project administration, funding acquisition, writing original draft; Philipp Harter – visualization, investigation; Mihails Kusnezoff – data discussion, manuscript revision; Teko W. Napporn – data discussion, manuscript revision; Hartmuth Schroettner – post-mortem analysis; Christoph Hochenauer – methodology, discussion and suggestions, analysis, writing – review and editing.

Conflicts of interest

There are no conflicts to declare.

Acknowledgements

Notes and references

1 S. Kahn Ribeiro, M. Josefi na Figueroa, F. Creutzig, C. Dubeux, J. Hupe, S. Kobayashi, L. Alberto de Melo Brettas, T. Thrasher, S. Webb and J. Zou, *Energy End-Use: Transport Convening Lead Authors (CLA) Lead Authors (LA) Contributing Authors (CA)*, 2012.

2 D. Papurello, A. Lanzini, S. Fiorilli, F. Smeacetto, R. Singh and M. Santarelli, *Chem. Eng. J.*, 2016, **283**, 1224–1233.

3 Y. Li, L. Na, Z. Li and S. Li, *Int. J. Hydrogen Energy*, 2020, **45**, 15650–15657.

4 F. Wang, H. Kishimoto, T. Ishiyama, K. Develos-Bagarinao, K. Yamaji, T. Horita and H. Yokokawa, *J. Power Sources*, 2020, **478**, 228763.

5 Z. Cheng, J.-H. Wang, Y. Choi, L. Yang, M. C. Lin and M. Liu, *Energy Environ. Sci.*, 2011, **4**(11), 4380–4409.

6 K. Sasaki, K. Haga, T. Yoshizumi, D. Minematsu, E. Yuki, R. Liu, C. Uryu, T. Oshima, T. Ogura, Y. Shiratori, K. Ito, M. Koyama and K. Yokomoto, *J. Power Sources*, 2011, **196**, 9130–9140.

7 D. Papurello and A. Lanzini, *Waste Manage.*, 2018, **72**, 306–312.

8 J. Bao, G. N. Krishnan, P. Jayaweera and A. Sanjurjo, *J. Power Sources*, 2010, **195**, 1316–1324.

9 K. Kuramoto, S. Hosokai, K. Matsuoka, T. Ishiyama, H. Kishimoto and K. Yamaji, *Fuel Process. Technol.*, 2017, **160**, 8–18.

10 Sunfire, *Energy Everywhere - Sunfire*, 2019, https://www.sunfire.de/en/.

11 Elcogen, *Elcogen - solid oxide cells and stacks*, 2020, https://elcogen.com/.

12 Y. Komatsu, G. Brus, S. Kimijima and J. Szmyd, *Appl. Energy*, 2014, **115**, 352–359.

13 Z. Wuillemin, S. Sa and D. Montinaro, *SOLIDpower stack technology development View project Production and Reliability Oriented SOFC Cell and Stack Design View project Cédric Beetschen SolidPower SA/HTceramix SA 6 PUBLICATIONS 15 CITATIONS SEE PROFILE*, 2014.

14 Q. Fang, L. Blum, R. Peters, M. Peksen, P. Batfalsky and D. Stolten, *Int. J. Hydrogen Energy*, 2015, **40**, 1128–1136.

15 V. Subotić, N. H. Menzler, V. Lawlor, Q. Fang, S. Pofahl, P. Harter, H. Schroettner and C. Hochenauer, *Appl. Energy*, 2020, **277**, 115603.

16 S. Futamura, A. Muramoto, Y. Tachikawa, J. Matsuda, S. Lyth, Y. Shiratori, S. Taniguchi and K. Sasaki, *Int. J. Hydrogen Energy*, 2019, **44**, 8502–8518.

17 S. Futamura, Y. Tachikawa, J. Matsuda, S. Lyth, Y. Shiratori, S. Taniguchi and K. Sasaki, *J. Electrochem. Soc.*, 2017, **164**, F3055–F3063.

18 V. Subotić, A. Baldinelli, L. Barelli, R. Scharler, G. Pongratz, C. Hochenauer and A. Anca-Couce, *Appl. Energy*, 2019, **256**, 113904.

19 K. Eguchi, H. Kojo, T. Takeguchi, R. Kikuchi and K. Sasaki, *Solid State Ionics*, 2002, **152–153**, 411–416.

20 R. Gorte, H. Kim and J. Vohs, *J. Power Sources*, 2002, **106**, 10–15.

21 R. Gorte and J. Vohs, *J. Catal.*, 2003, **216**, 477–486.

22 K. Girona, J. Laurencin, J. Fouletier and F. Lefebvre-Joud, *J. Power Sources*, 2012, **210**, 381–391.

23 J. Kihlman, J. Sucipto, N. Kaisalo, P. Simell and J. Lehtonen, *Int. J. Hydrogen Energy*, 2015, **40**, 1548–1558.

24 G. De Lorenzo and P. Fragiacomo, *Energy Convers. Manage.*, 2015, **93**, 175–186.

25 V. Subotić, C. Schluckner, J. Mathe, J. Rechberger, H. Schroettner and C. Hochenauer, *J. Power Sources*, 2015, **295**, 55–66.

26 Y. Wang, W. Shi, H. Li, M. Han and Z. Sun, *ECS Trans.*, 2019, **91**, 707–718.

27 T. Chen, W. G. Wang, H. Miao, T. Li and C. Xu, *J. Power Sources*, 2011, **196**, 2461–2468.

28 A. Lanzini, P. Leone, C. Guerra, F. Smeacetto, N. Brandon and M. Santarelli, *Chem. Eng. J.*, 2013, **220**, 254–263.

29 C. Schluckner, V. Subotić, V. Lawlor and C. Hochenauer, *J. Fuel Cell Sci. Technol.*, 2015, **12**, 051007.

30 W. Y. Lee, J. Hanna and A. F. Ghoniem, *J. Electrochem. Soc.*, 2013, **160**, 94–105.

31 K. Nikooyeh, R. Clemmer, V. Alzate-Restrepo and J. M. Hill, *Appl. Catal., A*, 2008, **347**, 106–111.

32 J. Kirtley, A. Singh, D. Halat, T. Oswell, J. M. Hill and R. A. Walker, *J. Phys. Chem. C*, 2013, **117**, 25908–25916.

33 V. Alzate-Restrepo and J. M. Hill, *J. Power Sources*, 2010, **195**, 1344–1351.

34 W. Y. Lee, J. Hanna and A. F. Ghoniem, *J. Electrochem. Soc.*, 2013, **160**, F94–F105.

35 K. Sasaki, *The Impact of Fuels on Solid Oxide Fuel Cell Anode Lifetime: The Relationship Between Fuel Composition, Fuel Impurities, and Anode Lifetime and Reliability*, Elsevier Ltd, 2017, pp. 37–50.

36 M. B. Pomfret, J. C. Owrutsky and R. A. Walker, *J. Electrochem. Soc.*, 2003, **150**, 271.

37 M. B. Pomfret, D. A. Steinhurst and J. C. Owrutsky, *J. Power Sources*, 2013, **233**, 331–340.

38 D. J. Cumming and R. H. Elder, *J. Power Sources*, 2015, **280**, 387–392.

39 J. D. Kirtley, D. A. Steinhurst, J. C. Owrutsky, M. B. Pomfret and R. A. Walker, *Phys. Chem. Chem. Phys.*, 2014, **16**, 227–236.

40 B. C. Eigenbrodt, M. B. Pomfret, D. A. Steinhurst, J. C. Owrutsky and R. A. Walker, *J. Phys. Chem. C*, 2011, **115**, 2895–2903.

41 Z. Tang, Q.-A. Huang, Y.-J. Wang, F. Zhang, W. Li, A. Li, L. Zhang and J. Zhang, *J. Power Sources*, 2020, **468**, 228361.

42 Q.-A. Huang, R. Hui, B. Wang and J. Zhang, *Electrochim. Acta*, 2007, **52**, 8144–8164.

43 B. Yang, J. Wang, M. Zhang, H. Shu, T. Yu, X. Zhang, W. Yao and L. Sun, *Energy Convers. Manage.*, 2020, **213**, 112856.

44 P. Costamagna, E. M. Sala, W. Zhang, M. Lund Traulsen and P. Holtappels, *Electrochim. Acta*, 2019, **319**, 657–671.

45 M. Saccoccio, T. H. Wan, C. Chen and F. Ciucci, *Electrochim. Acta*, 2014, **147**, 470–482.

46 F. Ciucci and C. Chen, *Electrochim. Acta*, 2015, **167**, 439–454.

47 T. H. Wan, M. Saccoccio, C. Chen and F. Ciucci, *Electrochim. Acta*, 2015, **184**, 483–499.

48 V. Subotić, B. Stoeckl, V. Lawlor, J. Strasser, H. Schroettner and C. Hochenauer, *Appl. Energy*, 2018, **222**, 748–761.

49 V. Subotić, B. Koenigshofer, D. Juricic, M. Kusnezoff, H. Schroettner, C. Hochenauer and P. Boškoski, *Energy Convers. Manage.*, 2020, **226**, 113509.

50 H. Sumi, T. Yamaguchi, K. Hamamoto, T. Suzuki, Y. Fujishiro, T. Matsui and K. Eguchi, *Electrochim. Acta*, 2012, **67**, 159–165.

51 E. Ramschak, V. Peinecke, P. Prenninger, T. Schaffer and V. Hacker, *J. Power Sources*, 2006, **157**, 837–840.

52 S. Thomas, S. C. Lee, A. K. Sahu and S. Park, *Int. J. Hydrogen Energy*, 2014, **39**, 4558–4565.

53 Q. Mao and U. Krewer, *Electrochim. Acta*, 2013, **103**, 188–198.

54 L. Malafronte, B. Morel and A. Pohjoranta, *Fuel Cells*, 2018, **18**, 476–489.

55 J. R. Wilson, D. T. Schwartz and S. B. Adler, *Electrochim. Acta*, 2006, 1389–1402.

56 S. Kavurucu Schubert and M. Kusnezoff, Effect of Operation Conditions on Soot Formation in SOFC Stacks, *ESC Meeting Abstract MA2009-02 1449*, vol. 2, 2019.

57 M. Kusnezoff, N. Trofimenko, M. Müller and A. Michaelis, *Materials*, 2016, **9**, 906.

58 V. Subotić, C. Schluckner, B. Stoeckl, M. Preininger, V. Lawlor, S. Pofahl, H. Schroettner and C. Hochenauer, *Energy Convers. Manage.*, 2018, **178**, 343–354.

59 C. Schluckner, V. Subotić, S. Preissl and C. Hochenauer, *Int. J. Hydrogen Energy*, 2019, **44**, 1877–1895.

60 S. McIntosh, J. M. Vohs and R. J. Gorte, *J. Electrochem. Soc.*, 2003, **150**, A470.

61 V. Subotić, C. Schluckner, M. Joerg, J. Rechberger, H. Schroettner and C. Hochenauer, *J. Power Sources*, 2015, **295**, 55–66.

62 C. Mallon and K. Kendall, *J. Power Sources*, 2005, **145**, 154–160.

63 Z. L. Zhang and X. E. Verykios, *Catal. Today*, 1994, **21**(2–3), 2589–3595.

64 M. Kennema and P. A. Rowntree, *J. Power Sources*, 2020, **453**, 226753.